Geochemistry 80 (2020) 125662

Contents lists available at ScienceDirect

Geochemistry

journal homepage: www.elsevier.com/locate/chemer

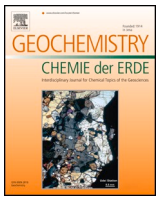

Late Cretaceous-Cenozoic exhumation of Northwestern Guangxi (China) and tectonic implications: Evidence from apatite fission track dating

Wu Jianbiao[a,b,c], Pi Qiaohui[a,d,*], Zhu Bin[a], Hu Yunhu[a], Li Guo[a,b], Wei Chaowen[a]

[a] Guangxi Key Laboratory of Hidden Metallic Ore Deposits Exploration, Guilin University of Technology, 541004 Guilin, China
[b] Faculty of Land Resource Engineering, Kunming University of Science and Technology, 650093 Kunming, China
[c] Southwest Institute of Geological Survey, Geological Survey Center for Nonferrous Metals Resources, 650093 Kunming, China
[d] State Key Laboratory of Ore Deposit Geochemistry, Institute of Geochemistry, Chinese Academy of Sciences, 550002 Guiyang, China

ARTICLE INFO

Handling Editor: Hongbo Zhao

Keywords:
Hydrothermal deposits preservation
Apatite fission track
Exhumation history
Northwestern Guangxi

ABSTRACT

The study of the Late Cretaceous-Cenozoic uplift and tectonic evolution of the Northwestern Guangxi area in the Youjiang Basin is relevant for understanding the origin and preservation of hydrothermal deposits with ore-hosting potential. Apatite fission-track dating and time-temperature thermal history modelling were performed using six rock samples from the study area. The ages were found to range from 14 to 81 Ma, and in particular, three distinct time intervals could be defined using the apatite fission-track ages: 81–77 Ma, 58–35 Ma, and 17–14 Ma, each corresponding to a specific tectonic-thermal event. The 81–77 Ma event indicates the age of early magmatic activity in northwestern Guangxi. The earliest Himalayan tectonic phase could be attributed to the subduction–collision of the Indo-Asian plate at 58–35 Ma, followed by a second phase of rapid wedging of the Indian plate during the 17–14 Ma interval. We surmise that some hydrothermal deposits, including medium-temperature Cu, Pb, Zn deposits and high-temperature W, Sn, Mo, Bi deposits such as polymetallic Cu–Fe–Mo, and Cu–Mo–(Pb–Zn) porphyry types and skarn types, may be locally present below the low-temperature Carlin-type gold deposits, or at variable depths in northwestern Guangxi. And sand gold deposits may be a relevant prospecting target.

1. Introduction

The Youjiang Basin is a late Palaeozoic–Mesozoic composite rift basin on the southwestern margin of the Yangtze Block. Since the late Palaeozoic, this block experienced a multiphase geodynamic evolution, along with the opening and spreading of the Palaeo-Tethys Ocean (Zhang et al., 2016). In particular, this region transformed from a rift basin to a passive continental margin and back arc basin during the Mesozoic–Cenozoic (Chen et al., 1993; Pi et al., 2015; Liang et al., 2011). Most of the hydrothermal deposits resulting from this complex tectonic evolution were formed in the Mesozoic (Hu et al., 2010). Northwestern Guangxi is an important part of the Yunnan–Guizhou–-Guangxi Golden Triangle region in the eastern domain of the Youjiang Basin (SW China), and it has a subduction and collision history spanning from the late Palaeozoic to present. This extensive geologic record is key to understanding the exhumation history of the Youjiang Basin, as well as assessing the preservation of hydrothermal deposits during the late Cretaceous–Cenozoic.

The subduction of the Indochina Block beneath the South China Block in the Mesozoic resulted in pervasive mineralisation events that resulted in diverse hydrothermal deposits within the South China Block (Hu et al., 2017a) (Fig. 1). Among these, the Dachang tin polymetallic ore field in northwestern Guangxi is a world-class super-large, high-temperature hydrothermal deposit related to the Yanshanian Longxianggai pluton (Chen et al., 1993; Pi et al., 2015; Liang et al., 2011). In addition, a series of Carlin-type gold deposits, similar to Mingshan and Bama, formed in a low-temperature hydrothermal environment (Kesler et al., 2005; Pi et al., 2017). These hydrothermal deposits show complete zoning with respect to the surrounding rocks (Cen and Tian, 2012; Mao et al., 2010; Zhang et al., 2012), centred on the rock masses. The zoning pattern displays a regular distribution from the inner zone to the middle and outer zones, compatible with a complete succession from high–intermediate and low temperature ore deposits, respectively (Cen and Tian, 2012; Mao et al., 2010; Zhang et al., 2012). Because the preservation of this zonation pattern is primarily controlled by uplifting and denudation, their reconstruction is essential for defining the occurrence and nature of hydrothermal deposits and ore districts (Yuan, 2016).

* Corresponding author at: Guangxi Key Laboratory of Hidden Metallic Ore Deposits Exploration, Guilin University of Technology, 541004 Guilin, China.
E-mail address: 1481561260@qq.com (Q. Pi).

https://doi.org/10.1016/j.chemer.2020.125662
Received 3 September 2019; Received in revised form 12 May 2020; Accepted 18 May 2020
Available online 24 May 2020
0009-2819/

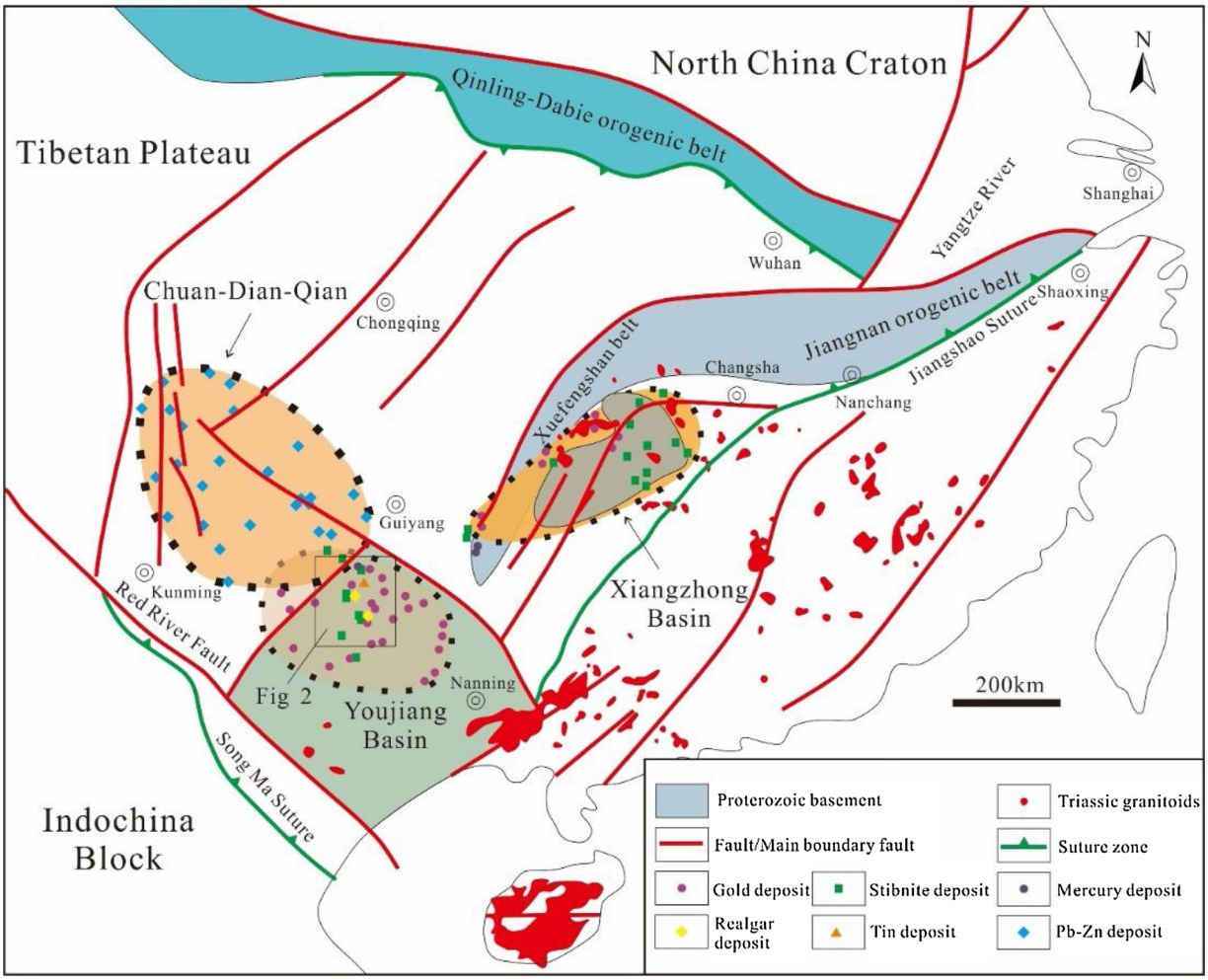

Fig. 1. A simplified geological map of the South China Block and adjacent regions showing the structural framework and the distribution of ore deposits in the Yangtze Block (modified from Hu et al., 2017a; Qiu et al., 2016).

Fission track thermochronology, a frontier methodology in geochronology, has proven to be particularly advantageous in reconstructing the long term (millions of years) thermal history of the upper crust based on carrier minerals, such as zircon and apatite (Yuan, 2016; Feng et al., 2017; Piedrahita et al., 2017). Fission track thermochronology is widely used to study of igneous, metamorphic, and sedimentary rocks, with regard to their formation, duration of thermal processes, and tectonic setting of altered rock masses (Leng et al., 2018; Lei et al., 2008). The characteristics of apatite fission track dating and track length distribution provide quantitative information on cooling through partial annealing (PAZ) of rocks, and record the thermal history of rocks within a range of 110–60 °C. This change in thermal environment is generally considered the result of regional uplift and/or denudation (Green, 1981; Qiu et al., 2016). By simulating the geological thermal history, along with estimates of uplift/denudation and rough evaluation of the state of preservation and alteration of deposits, a theoretical frame can be reconstructed as a basis for predicting mineral resources and metallogenic potentials (Yuan. 2016; Feng et al., 2017; Wang et al., 2017).

In this paper, we report the first study of apatite fission track thermochronology of northwestern Guangxi. We present six new apatite fission track ages determined using various samples collected in northwestern Guangxi. Along with the modelling of the thermal history, we aimed to constrain the late Cretaceous–Cenozoic tectono-thermal evolution of northwestern Guangxi. The findings also provide deeper insight into the role of exhumation and denudation in the thermal history and preservation of zoned hydrothermal deposits.

2. Geological background

2.1. Regional geological setting

The South China Block includes the Yangtze Block to the northwest and the Cathaysia Block to the southeast (Hu et al., 2017a) (Fig. 1). The southwestern margin of the Yangtze Block in northwestern Guangxi hosts the Youjiang Basin, a sector of the late Palaeozoic Palaeo-Tethys and Pacific structural domain (Peng and Lu, 2019). The southwestern margin of this area is connected to the Red River Fault and the Indosinian Block. The southeastern and eastern margins are bounded by the Pingxiang-Nanning-Kunlunguan Fault and the Nandan-Duan Fault, respectively, and include the Baiwandashan Fault depression and the central Guizhou depression. The western and northern boundaries are controlled by the Mile-Shizong Fault, Shuicheng-Ziyun-Bama Fault, and eastern part of the Nanpanjiang Fault; these are also connected to the Yangtze platform and represent the boundary between the Yangtze Block and the South China geosyncline (Hu et al., 2017a) (Fig. 1).

The oldest lithologic units in the Youjiang Basin are Cambrian carbonate rocks and early Palaeozoic clastic rocks that crop out along the core of an anticline (Qiu et al., 2016). The Youjiang Basin has been suggested to overlie a basement of Lower Palaeozoic strata and to have evolved in three stages: 1) rift basin to passive continental margin; 2) back arc basin; and 3) foreland basin. These stages correspond to the opening, subduction, and closing of the Palaeo-Tethys ocean, respectively (Chen et al., 2015; Hu et al., 2017a). The sedimentary cover of the Youjiang Basin consists mainly of a thick Permo-Triassic marine

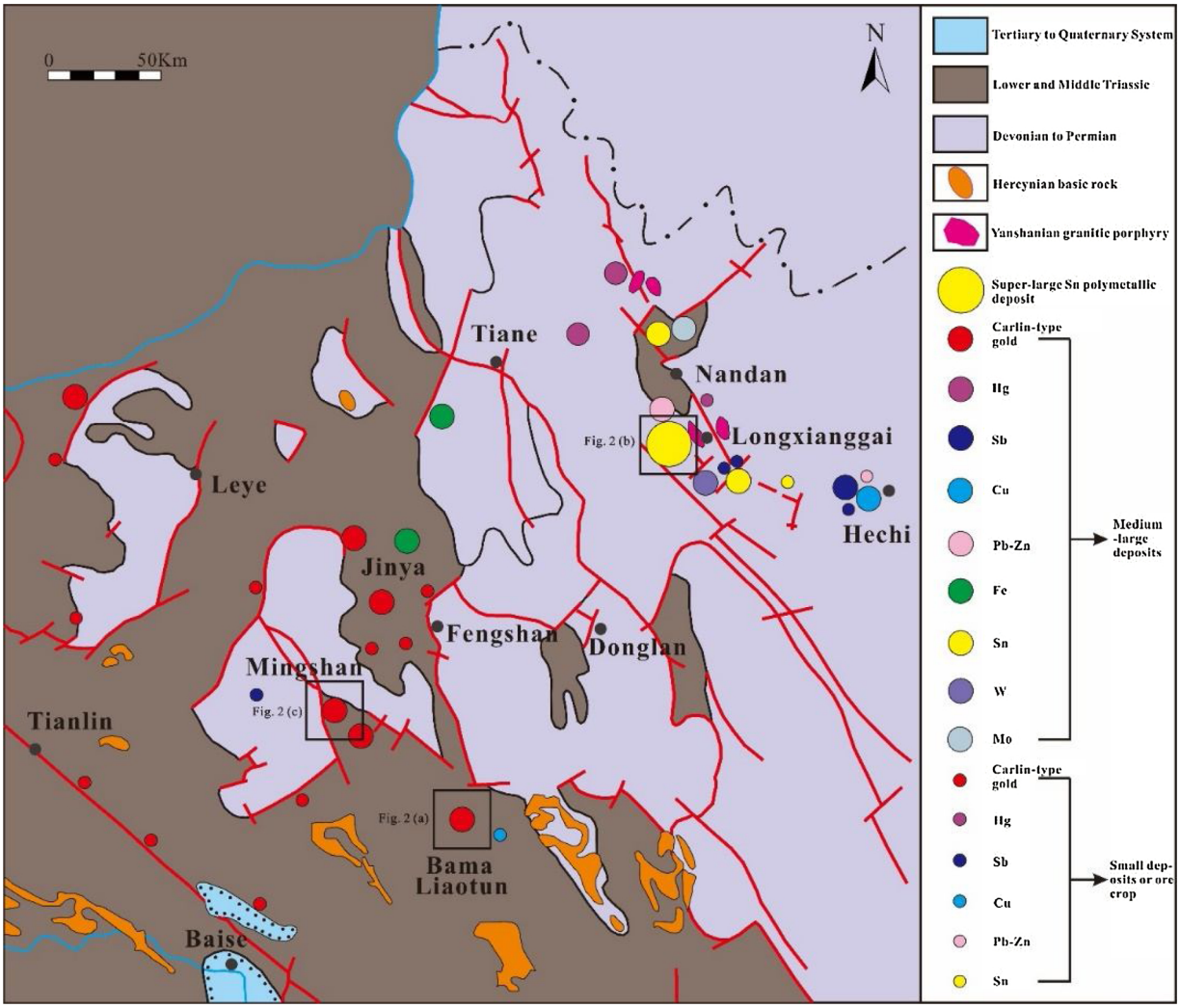

Fig. 2. Schematic geological map and Mineral distribution map of the Northwest Guangxi (modified from Guo, 1994).

succession, composed of limestones, dolostones, siltstones, sandstones, and mudstones, variably cropping out in the basin (Fig. 2). In addition, Indosinian diabase intrusions are known in the southern part of the basin, which have been interpreted as the western-most manifestation of the Emeishan mantle plume. The occurrence of Indosinian granitic intrusions deep in the Youjiang Basin are inferred from geophysical evidence (Zhou, 1993).

The Youjiang Basin is rich in mineral resources which are widely distributed. A large number of low-temperature Carlin-type gold deposits are developed in this area, including Bama Carlin-type gold deposits and Mingshan Carlin-type gold deposits; while high-temperature deposits are mainly Sn polymetallic deposits, among which Dachang Sn polymetallic ore field is the typical representative (Fig. 2).

2.2. Lithologic and mineralogic composition of deposits

2.2.1. Bama Carlin-type gold deposit

The Bama Carlin-type gold deposit in northwestern Guangxi is located in the area extending from Suoluo Township (Bama County) to Yuyatun (Baijiucun Village). The mining area lies within a monoclinal fold structure. The strata strike NW and are inclined toward the NE or SW. Nine faults have been identified in the mining area, of which the NW-trending ones are synsedimentary; both NW-trending and nearly EW-trending faults are ore-controlling and ore-hosting faults (Chen et al., 2014; Li et al., 2014a) (Fig. 3a). Outcrops in the mining area include Carboniferous, Permian and Triassic clastic deposits, and exposed magmatic rocks are mainly quartz porphyry. The main ore-bearing rocks consist of deep-water sandstone–mudstone alternations deposited around an isolated carbonate platform comprising Carboniferous limestones with intercalated dolomite and Permian sponge reef limestones (Chen et al., 2014; Li et al., 2014a). At present, five gold ore bodies have been found in the mining area, referred to as I-1, I-2, III, IV, and V ore bodies. The ore bodies are vein-like and/or lenticular in shape and occur as infill deposits of fractures affecting Triassic strata. The ore deposits consist mainly of silicified and limonized sandstones, cataclastic sandstones, argillaceous siltstones and, locally, quartz porphyry. The surrounding rocks mainly belong to the Baifeng Formation and include mudstones and silty mudstones (Li et al., 2014a). The quartz porphyry from a dyke with a NE strike dissecting the core of the Longtan anticline. The $^{40}Ar/^{39}Ar$ dating of muscovite phenocryst from quartz porphyry veins yielded a plateau age of (95.5 ± 0.7) Ma (Chen et al., 2014). This quartz porphyry cuts the ore body and strata, and the ore body is produced along the stratum.

2.2.2. The Mingshan Carlin-gold deposit

The Mingshan Carlin-type gold deposit in northwestern Guangxi is part of a continental margin clastic succession located on the southwest flank of the Bahe platform (an anticline structure) in the central part of the Youjiang basin (Pang et al., 2014; Li et al., 2015). The mining area is affected by two main fault systems exhibiting a NW or NE trend. The NW-trending faults, which likely control the orientation of the ore bodies, are larger in scale with a compressive-torsional

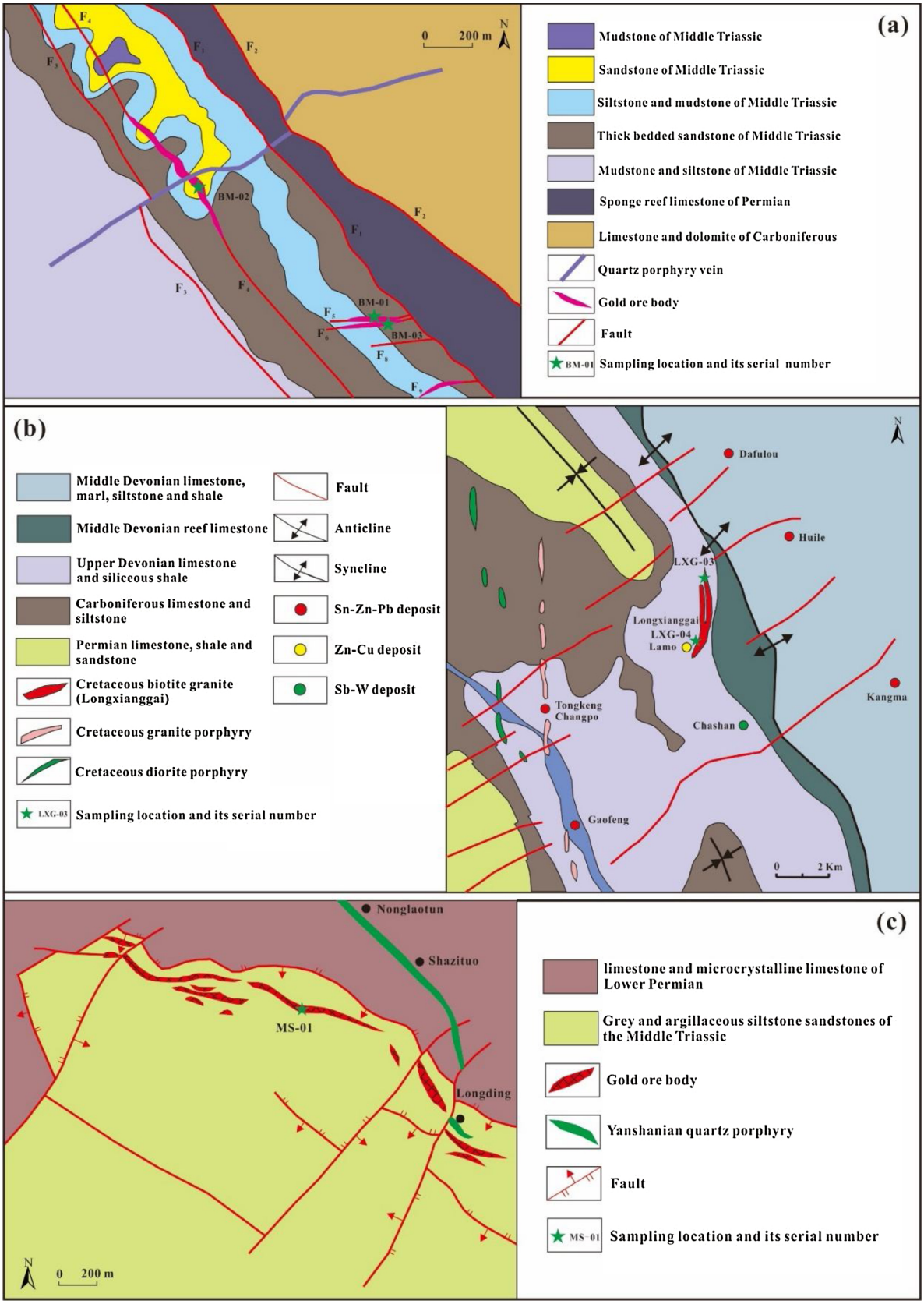

Fig. 3. Deposit geology and sample distribution map (Modified after Chen et al., 2014; Guo et al., 2018; Pang et al., 2014).

kinematic and well developed secondary structures; the NE-trending faults are smaller in scale and displace the NW-trending faults, indicating their younger age (Pang et al., 2014; Chen et al., 2012; Hu et al., 1995) (Fig. 3c). The strata exposed in the mining area include shallow-water, thick-bedded grey limestones, lower Permian microcrystalline limestones, and Middle Triassic and moderately thick

argillaceous siltstones with thin-bedded mudstones (Pang et al., 2014; Chen et al., 2012; Hu et al., 1995; Li et al., 2015). Among these, the Middle Triassic strata are the most important ore-bearing strata. In addition, Yanshanian quartz porphyry occurs in the northern and eastern parts of the mining area (K-Ar age is 80.9–84.9 Ma) (Pang et al., 2014). Hydrogen, oxygen, and argon isotopes from fluid inclusions, as well as the chemical composition of the quartz porphyry, indicate that its mineralisation may be related to magmatic activity (Hu et al., 1995). The NW-trending faults control the ore bodies and induce a parallel trend in the orientation of layers, veins, and lenses, typically concentrated in fault fracture zones. These bodies prevalently yield primary ores with scattered pyrite and arsenopyrite. The observed types of hydrothermal alteration and metallogenic stages are comparable with those of other similar deposits and consist of silicification, clayization, pyritization, and arsenopyritisation as the main mineralisation processes; these are occasionally associated with realgarization and stibium mineralisation. Arsenic-bearing pyrite is the main gold-bearing mineral (Chen et al., 2012); gold is for the most part distributed in the outer ring of arsenic-rich pyrite, in micro- or sub-micro form (Chen et al., 2009).

2.2.3. The Dachang Sn polymetallic ore field

The Dachang Sn polymetallic ore field is located southwest of the Jiangnan block, which is the transition zone between the Yangtze landmass and Cathaysia plate active belt. The Danchi fault dissects the eastern part of the ore field (Chen et al., 1993; Pi et al., 2015; Cai et al., 2006). The Longxianggai pluton, located in the central part of the Dachang tin ore field, is the largest intrusive body in this area. It is located in the structural high along the junction between the NW-trending Danchi fold belt and a NE-trending fault structure (Liang et al., 2011; Chen et al., 1993). According to the spatial relationship between the tectonic structures and the deposit, the Dachang ore field can be divided into three ore belts: the western ore belt, central ore belt, and eastern ore belt. The western ore belt is located in the Dachang fault zone, which in greater part comprises the Dachang fault and the associated NW-trending Dachang anticline. This fold-fault zone controls the cassiterite-sulphide deposits in Changpo-Tongkeng, Bali, and Longtoushan (Cai et al., 2006; Liang et al., 2011; Pi et al., 2015) (Fig. 3b). Late Palaeozoic and Mesozoic strata are dominant in this area, and horizons hosting the tin polymetallic ore are primarily found within Devonian strata. Copper is associated only with calcite quartz veins of later formations, whereas lead and zinc occur within Carboniferous and Permian strata, although at concentrations not relevant for industrial-scale exploitation. The Middle Devonian strata in the central ore belt, western ore belt, and Beixiang area of the Dachang ore field consist of black mudstones, shales, reef limestones, siltstones, and muddy sandstones. The Upper Devonian strata include siliceous rocks, striped limestones, lentil limestones, marlite calcareous shales, sandstones, and carbonaceous shales. These units occur on the flanks of the Danchi anticline and represent the main ore-bearing strata of the Danchi metallogenic belt. Evidence of magmatic activity in the Danchi metallogenic belt is relatively common and can be referred essentially to the granitic magmatic activity during the middle and late Yanshanian period. It is characterised by the intrusion of intermediate-acid magma and the formation of biotite granite, granite porphyry, quartz diorite porphyry, quartz porphyry, dacite porphyry, granite, and a minor amount of diabase porphyry (Pi et al., 2015; Chen et al., 1993; Liang et al., 2011). The Longxianggai complex pluton is the largest pluton in the middle of Dachang Sn polymetallic ore field. Its main body is biotite granite, which is experienced three stages of magmatic intrusion. The metallogenic age of Dachang Sn polymetallic ore field is closely related to magmatic intrusion in the early Cretaceous (120–100 Ma) (Wu et al., 2020).

3. Sample collection and characterisation

Six samples were collected from the Bama Carlin-type gold deposit, Mingshan Carlin-type gold deposit, and Dachang Sn polymetallic ore field. The locations of the sampling sites are presented in Fig. 3. In the Bama Carlin-gold ore body (Fig. 3a), three samples were collected from gold ore body No. III close to the F_5 EW fault zone (BM-01), gold ore body No. I- 2, a silicified ferritized rock in the fracture zone of F_4 and the surrounding area (BM-02), and gold ore body No. IV in the fracture zone of F_6, along the EW strike of the ore body (BM-03). In the Mingshan Carlin-type gold deposit, one sample (MS-01) was collected from the Carlin-gold ore body at a depth of 684 m below ore body No. 2 (Fig. 3c). In the Dachang tin polymetallic ore field, samples LXG-03 and LXG-04 were collected from the biotite-granite of the Longxianggai complex pluton (Fig. 3b).

4. Methods and approach

Apatite concentrates were extracted from crushed rock samples by using standard techniques. These techniques require that samples are comminuted to a particle size suitable to the size of the minerals in the rock, usually about 60 meshes. After coarse separation by traditional methods, samples were separated by using the conventional techniques of crushing, magnetic, and heavy-liquid separation. Samples of apatite were then mounted on glass slides using epoxy glue, polished and etched in 7% HNO_3 for 30 s at 25 °C to reveal the spontaneous fission-tracks. Neutron fluence was monitored with the CN_5 uranium dosimeter glasses for apatite samples (Yuan et al., 2009; Feng et al., 2017; Tang et al., 2018). The fission-track length and the spontaneous and induced track densities were measured by selecting cylinders parallel to the c-axis with an AutoSCAN system.

The IUGS-recommended Zeta calibration approach was used to calculate the central fission-track ages (Yuan et al., 2009; Feng et al., 2017; Tang et al., 2018); errors were also calculated (Green, 1981). The Zeta value for apatite is 410.4 ± 17.6. According to the technical error given by Green (1981), χ^2 is used to evaluate the probability of a single particle belonging to a particular age group. Values of $P(\chi^2) > 5\%$ indicate that fission-track samples contain a population (Yuan et al., 2009; Feng et al., 2017; Tang et al., 2018) with a single age. On the contrary, values of $P(\chi^2) < 5\%$ provide evidence for over dispersion, the extent of which is indicated by the percentage of dispersion around the central age.

5. Results and interpretation

5.1. Apatite fission-track analysis

Apatite fission track data for the six samples are reported in Table 1 and plotted in Fig. 5. The individual ages from three samples had $P(\chi^2)$ values greater than 5%, indicating that they form a single age group; those from the other three samples failed the χ^2-test ($P(\chi^2) < 5\%$), indicating that the single ages in the samples are dispersed and of mixed ages.

Therefore, we divided the samples into two groups. The first group comprised BM-01, BM-02, and BM-03, which passed the χ^2-test ($P(\chi^2) > 5\%$). We used the central ages for these samples: 49 ± 7 Ma (BM-01), 56 ± 5 Ma (BM-02), and 58 ± 7 Ma (BM-03). The average track length in these samples ranged from 12.3 ± 2.6 μm to 14.4 ± 0.5 μm (Table 1, Fig. 4). The second group comprised samples MS-01, LXG-03, and LXG-04, which failed the χ^2-test ($P(\chi^2) < 5\%$); the normal distribution was not followed. BinomFit software (Brandon, 1996) was used to decompose the fission-track age data, as shown in Fig. 5. Results of BinomFit decomposition showed that the samples could be decomposed into three age groups, except for MS-01 and LXG-03. Nevertheless, sample LXG-04 could be decomposed into two age groups (Fig. 4). As shown in Fig. 4, sample MS-01 has a central age of 39 ± 4

Table 1
Fission-track ages of apatite from the golden triangle region, SW China using an external detector method and zeta calibration approach.

Sample	Lithology	N	ρs (10^5/cm^2)(Ns)	ρi (10^5/cm^2)(Ni)	ρd (10^5/cm^2)(N)	P(χ^2)(%)	Central age (Ma)(± 1σ)	Pooled age (Ma)(± 1σ)	L(μm)	Number of Lengths
Bama										
BM-01	ore body	33	0.685(61)	3.155(281)	11.123(8116)	100	49 ± 7	49 ± 7	14.4 ± 0.5	3
BM-02	ore body	28	0.818(288)	3.674(1293)	12.344(8116)	62.3	56 ± 5	56 ± 4	12.8 ± 2.0	105
BM-03	ore body	27	0.684(93)	3.082(419)	12.675(8116)	99.5	58 ± 7	58 ± 7	12.3 ± 2.6	20
Mingshan										
MS-01	ore body	28	2.478(458)	15.627(2888)	12.006(8116)	0	39 ± 4	39 ± 3	12.5 ± 1.9	107
Longxianggai										
LXG-03	biotite-granite	25	5.315(1920)	23.045(8325)	13.226(8116)	0	60 ± 4	62 ± 3	13.1 ± 2.2	128
LXG-04	biotite-granite	7	3.026(235)	23.308(1810)	12.006(8116)	0.4	30 ± 4	32 ± 3	12.4 ± 1.7	18

Note: Track densities (ρ) are as measured and are (10^5per cm^{-2}) number of grains counted (n) are shown in parentheses. P(χ^2) is chi-square probability. Apatite ages calculated with ζ (zeta) = 410.4 ± 17.6(yr cm^2/tr).

Ma (Table 1, Fig. 4). The 27 individual apatite fission track ages range between 7.04 Ma and 87.93 Ma. Three age populations with Gaussian distributions were distinguished by the BinomFit decomposition, suggesting three ages of 14.2 Ma, 40.8 Ma, and 81.6 Ma (Fig. 5), with the middle being dominant. Twenty-four apatite crystals analysed from sample LXG-03 yielded a central age of 60 ± 4 Ma (Table 1, Fig. 4). The individual apatite fission track ages could be clearly separated into three populations of ca. 35.2 Ma (P1), 54.2 Ma (P2), and 77.1 Ma (P3) (Fig. 5), with the middle and latter being dominant. Apatite fission track analyses of six apatite crystals from sample LXG-04 yielded a central apatite fission track age of 30 ± 4 Ma (Table 1, Fig. 4), which apparently shows the provenance signal. Results of BinomFit decomposition showed two normally distributed age populations of ca. 17.0 Ma (P1) and 37.3 Ma (P2), with the latter being dominant. Apatite fission tracks with P(χ^2) values under 5% yielded mean lengths ranging from 12.4 ± 1.7 μm to 13.1 ± 2.2 μm.

A track-age histogram was constructed incorporating the decomposed age where the χ^2-test gave P(χ^2) < 5% and the central age where the χ^2-test gave P(χ^2) > 5% to reflect the distribution of and changes in the ages of the samples (Fig. 6). As shown in Fig. 6, apatite fission track ages range between 81.6 Ma and 14.2 Ma and can be divided into three groups: 81.6–77.1 Ma, 58–35.2 Ma, and 17–14.2 Ma.

5.2. Thermal history

HeFTy software (Ketchman, 2005) was used to model thermal history on the basis of the distributions of apatite fission-track lengths and apatite fission track age data. To interpret the significance of our data better, we modelled all of the apatite fission track data to quantify the thermal history and regularity of mineralisation in the Carlin-type gold deposits of northwestern Guangxi. Only samples with sufficient numbers of measured confined tracks (BM-02, MS-01, and LXG-03) were used in the modelling. Where applicable, the initial apatite fission track length adopted for the modelling was based on sample D_{par} values. The apatite fission track data and present-day surface temperature were incorporated as additional constraints on the thermal history (Fig. 8). The models for all the three samples are illustrated in Supplementary Fig. 8. Fig. 8 shows that the ages of all of the samples had a goodness of fit of over 0.93, showing that the simulation results are of high quality. The modelling revealed that the sample apatite fission track data, except for sample BM-02, can be explained by a three-stage cooling history (Supplementary Fig. 8). The modelling results suggest cooling in the northwestern Guangxi region since 90 Ma. This corresponds to the thermal evolution of fission-tracks in three samples illustrated in Fig. 7. We assumed a geothermal gradient of 35 ℃/km and used this value to calculate the exhumation rate of northwestern Guangxi (Wang et al., 1986).

The simulation of the thermal history of apatite fission track in sample BM-02 revealed five phases of cooling and exhumation. The first stage was a phase between 87 Ma and 48 Ma, with barely any cooling. The second stage was a phase of rapid cooling between 48 Ma and 42 Ma. The temperature dropped rapidly from ~90 ℃ to ~56.6 ℃, giving an average cooling rate of 5.567 ℃/Ma and an uplift rate of 0.159 mm/a. The amount of exhumation was 0.954 km, indicating the action of an intense and rapid process. After this stage of rapid cooling came a period of slow continuous cooling from ca. 42 Ma to 18.3 Ma. The temperature dropped from ~56.6 ℃ to ~49.2 ℃, with an average cooling rate of 0.312 ℃/Ma and an uplift rate of 0.009 mm/a. The amount of exhumation was 0.211 km. The fourth stage represents another phase of rapid cooling between 18.3 Ma and 10.7 Ma. The temperature dropped rapidly from ~49.2 ℃ to ~19.7 ℃, giving an average cooling rate of 3.882 ℃/Ma and an uplift rate of 0.111 mm/a. The amount of exhumation was 0.843 km, indicating the action of an intense and rapid process. The last stage was a phase of slow cooling between 10.7 Ma and 0 Ma. The temperature dropped from ~19.7 ℃ to ~18.7 ℃, with an average cooling rate of 0.093 ℃/Ma and an uplift

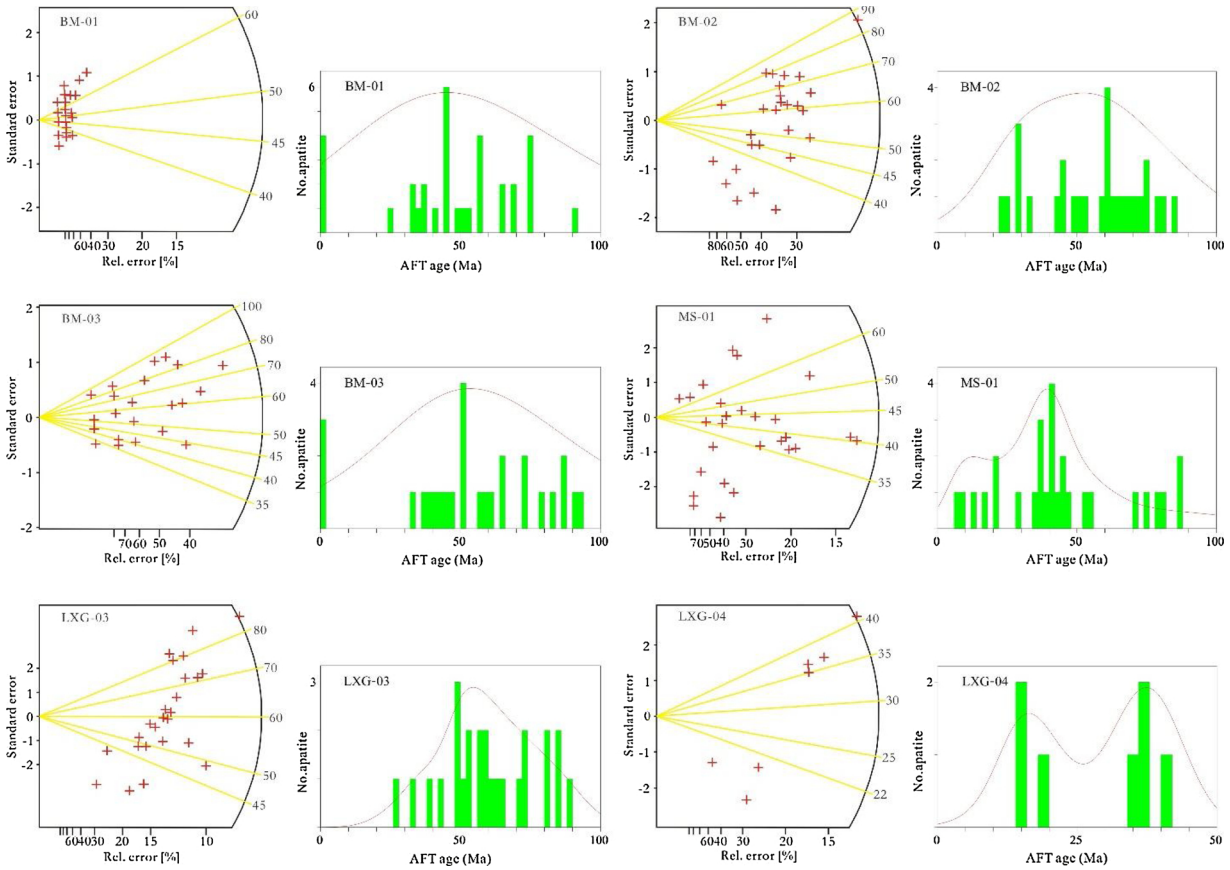

Fig. 4. Radial plots with abanico curves and Histograms of apatite fission-track data drawn with Radial Plotter program (Vermeesch, 2009). Each dot represents a crystal; the age can be read on the intersection between a line linking the origin with a dot and the arc; the precision in age is reported on the x axis. Bars on the y axis indicate the standard error of each measurement.

rate of 0.003 mm/a. The amount of exhumation was 0.029 km. Thus, the total amount of exhumation in the area of the Bama Carlin-type gold deposit after 90 Ma is 2.037 km. The Bama gold deposit appears to have experienced two rapid uplifting stages: 48 to 42 Ma in the second stage and 18.3–10.7 Ma in the fourth stage.

The simulated thermal history of apatite fission track in sample MS-01 was similar to that of sample BM-02, with five phases of cooling and exhumation. The first stage was a phase of slow cooling between 85.5 Ma and 49.7 Ma. The temperature dropped from ~118.2 ℃ to ~110.6 ℃, with an average cooling rate of 0.212 ℃/Ma and an uplift rate of 0.006 mm/a. The amount of exhumation was 0.217 km. The second stage was a phase of rapid cooling between 49.7 Ma and 36.8 Ma. The temperature dropped rapidly from ~110.6 ℃ to ~71.8 ℃, giving an average cooling rate of 3.008 ℃/Ma and an uplift rate of 0.068 mm/a. The amount of exhumation was 1.109 km, indicating the action of an intense and rapid process. This stage was followed by a period of slow continuous cooling from ca. 36.8 Ma to 12.4 Ma. The temperature dropped from ~71.8 ℃ to ~65 ℃, with an average cooling rate of 0.279 ℃/Ma and an uplift rate of 0.008 mm/a. The amount of exhumation was 0.194 km. Another phase of rapid cooling occurred in the fourth stage between 12.4 Ma and 5.6 Ma. The temperature dropped rapidly from ~65 ℃ to ~20.5 ℃, with an average cooling rate of 6.544 ℃/Ma and an uplift rate of 0.187 mm/a. The amount of exhumation was 1.271 km, indicating the action of an intense and rapid process. The last stage was a phase of slow cooling between 5.6 Ma and 0 Ma. The temperature dropped from ~20.5 ℃ to ~19.7 ℃, with an average

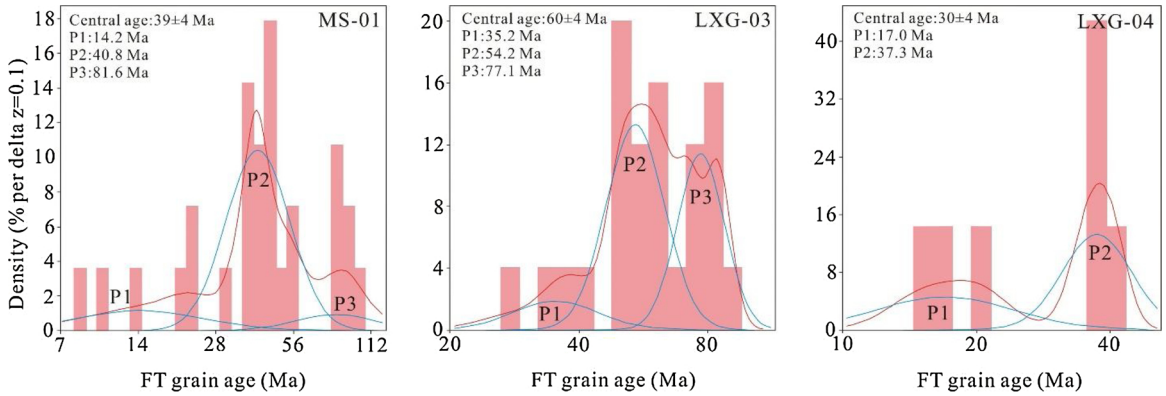

Fig. 5. Age probability densities (Brandon, 1996) of Apatite fission-track age group with P(χ^2) < 5%.Within probability density plots, the blue thin lines indicate the peak ages within one sample.

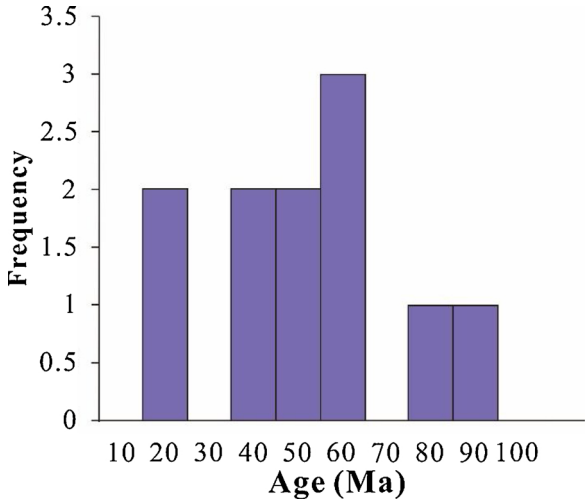

Fig. 6. Distribution histogram of apatite fission-track.

cooling rate of 0.143 ℃/Ma and an uplift rate of 0.004 mm/a. The amount of exhumation was 0.023 km. Thus, the total amount of exhumation in the area of the Mingshan Carlin-type gold deposit after 90 Ma is 2.814 km. Thus, the Mingshan gold deposit experienced two rapid uplifting stages: 49.7–36.8 Ma in the second stage and 12.4–5.6 Ma in the fourth stage.

The simulation of the thermal history of apatite fission-tracks in sample LXG-03 revealed four cooling and exhumation phases. The first stage was a phase between 68.8 Ma and 60.8 Ma, with barely any cooling. The second stage from ca. 60.8 Ma to 40 Ma experienced a relatively rapid temperature drop from ~88 ℃ to ~73.8 ℃, accounting for an average cooling rate of 0.683 ℃/Ma and an uplift rate of 0.02 mm/a. The amount of exhumation was 0.406 km, corresponding to an intense and rapid event. The stage of rapid cooling was followed by a phase of very rapid and continuous cooling from ca. 40–38 Ma, during which the temperature dropped from ~73.8 ℃ to ~31.2 ℃, with an average cooling rate of 21.3 ℃/Ma. The uplift rate was 0.609 mm/a, and the amount of exhumation was 1.217 km. Unlike the previous two deposits, an episode of continuous cooling occurred 38 Ma later, during which the temperature dropped from ~31.2 ℃ to ~18.5 ℃. The average cooling rate was 0.334 ℃/Ma, uplift rate was 0.010 mm/a, and amount of exhumation was 0.363 km. Thus, the total amount of exhumation in the Longxianggai area after 90 Ma is 1.986 km. The Longxianggai area appears to have experienced two rapid uplifting stages: 60.8–40 Ma in the second stage and 40 to 38 Ma in the third stage.

6. Discussion

6.1. Exhumation history of the northwestern Guangxi

Northwestern Guangxi is an important part of the Golden Triangle region hosting Carlin-type gold deposits (Cai and Zhang, 2009; Lepvrier et al., 2011; Yang et al., 2012; Faure et al., 2014; Chen et al., 2015; Qiu et al., 2016). These gold deposits are located in the Youjiang Basin, which lies in the southwestern part of the South China block (Chen et al., 2015). The Youjiang Basin is bounded by the Ziyun-Luodian fault to the northeast and Shizong-Mile fault to the northwest, and extends to the southwest reaching the northeastern Vietnam nappes (Cai and Zhang, 2009; Lepvrier et al., 2011; Yang et al., 2012; Faure et al., 2014; Qiu et al., 2016). Previous studies have focused on the age of metallogenic Carlin-type gold deposits in the Golden Triangle region. The genesis and evolution of the Carlin-type gold deposit is generally well constrained, and numerous isotopic dating methods, such as Rb-Sr and Re-Os of sulphides, and ^{40}Ar-^{39}Ar of sericite, have been applied (Hu et al., 1995, 2002; Su et al., 1998, 2009; Chen et al., 2009, 2015). The available data indicate that the Carlin-type gold deposits in the Youjiang Basin were formed during 235–200 Ma and 150–130 Ma (Su et al., 2009; Wang et al., 2013; Peng et al., 2003; Hu et al., 1995; Chen et al., 2015; Hu et al., 2017a; Pi et al., 2016, 2017).

It has been proposed that the Indosinian magmatism and mineralisation took place during the collision between the Indochina Block and the South China Craton, resulting in the closure of the Palaeo-Tethys (Wang et al., 2004, 2007; Qiu et al., 2016). Within this interval, mineralisation occurred prevalently during the Indosinian stage (235–200 Ma) (Wang et al., 2013; Gao et al., 2016; Hu and Zhou, 2012; Hu et al., 2017a, b; Pi et al., 2016). Alternatively, it has been suggested that the Yanshanian (150–130 Ma) was the main metallogenic period, corresponding to the late stages of the Yanshanian Orogeny (Su et al., 2009; Wang et al., 2013; Peng et al., 2003).

Regional scale fluid migration was initiated and largely influenced by orogenic events. The large-scale migration occurred along deep-seated regional faults, during which an ore-forming fluid rich in metal elements was generated by the continuous leaching and extraction of the basement rocks or sedimentary caprock. Then the ore-forming fluid penetrated along the deep faults. Atmospheric precipitation leached the rocks of the basin and extracted the reductive brine in the formation. Magmatic activity during the orogenetic process enhanced the extensive circulation of atmospheric precipitation (Hu et al., 2017a; Pi et al., 2016). The two kinds of fluids flowed in different parts of the structure to form the deposit. These include high-temperature W–Sn, polymetallic Cu–Fe–Mo, Cu–Mo–(Pb–Zn) porphyry types, low-temperature MVT-type Pb–Zn–Ag, Carlin-type Au, vein-type Sb, Hg, and As deposits (Hu and Zhou, 2012; Hu et al., 2017a,b; Pi et al., 2016).

In addition, some researchers have associated the Carlin type gold deposits in Yunnan, Guizhou, and Guangxi with magmatic activity in the late Yanshanian period (110 − 80 Ma) and inferred that lithospheric extension and thinning provide a tectonic setting favourable for metallogenic processes (Hu et al., 2002; Zhu et al., 1998; Mao et al., 2004; Mao et al., 2012; Zhang and Yang, 1992; Su et al., 1998). In fact, the Indosinian (235–200 Ma) and Yanshanian (150–130 Ma) metallogeny were overprinted by the Late Yanshanian (110–80 Ma) ore deposits (Yang et al., 2008; Cheng et al., 2010; Zhang et al., 2003; Liu and Hua, 2005; Hu and Zhou, 2012; Jia and Hu, 2001; Hu et al., 2017a). The superimposition can be divided into three stages: ore leaching, migration and enrichment, and ore precipitation and enrichment. The first is controlled by mineralisers and the last by precipitants (Jia and Hu, 2001). In the stage of leaching, migration, and enrichment, the mineraliser selectively extracts metal elements to form concentrated ore-bearing fluids that enrich rocks in weak structural zones and in the lower part of argillaceous barriers. The differentiation of reductive fluids in the basin, invasion of mantle derived basic dykes along structurally fragile zones, and enhancement of hydrothermal maturation of organic matter mark the onset of the stage of sedimentation and enrichment. The increase of reductive precipitants and the decomposition of organic matter in the structurally fragile zones change the physical and chemical conditions of the metal rich fluids in the migration state and destroy the stability of the metal complex. Therefore, metal ions can be reduced to natural metals or combined with reductive precipitants to form sulphides and arsenides (Jia and Hu, 2001).

Thus, the continuous action of tectonic thermal events before the late Yanshanian allowed the deposit to reach a stable stage in the late Yanshanian. Our apatite fission tracks record the ages of the first thermal events as 81.6–77.1 Ma. On this basis, we modelled all available apatite fission track data to quantify the thermal history and regularity of mineralisation in the Carlin-type gold deposits of the Golden Triangle region. The results of thermal history modelling for northwestern Guangxi clearly reveal uplift and exhumation since the late Yanshanian (90 Ma).

The thermal event at 81.6–77.1 Ma recorded by sample LXG-03 likely indicates the age of formation of the main body of the

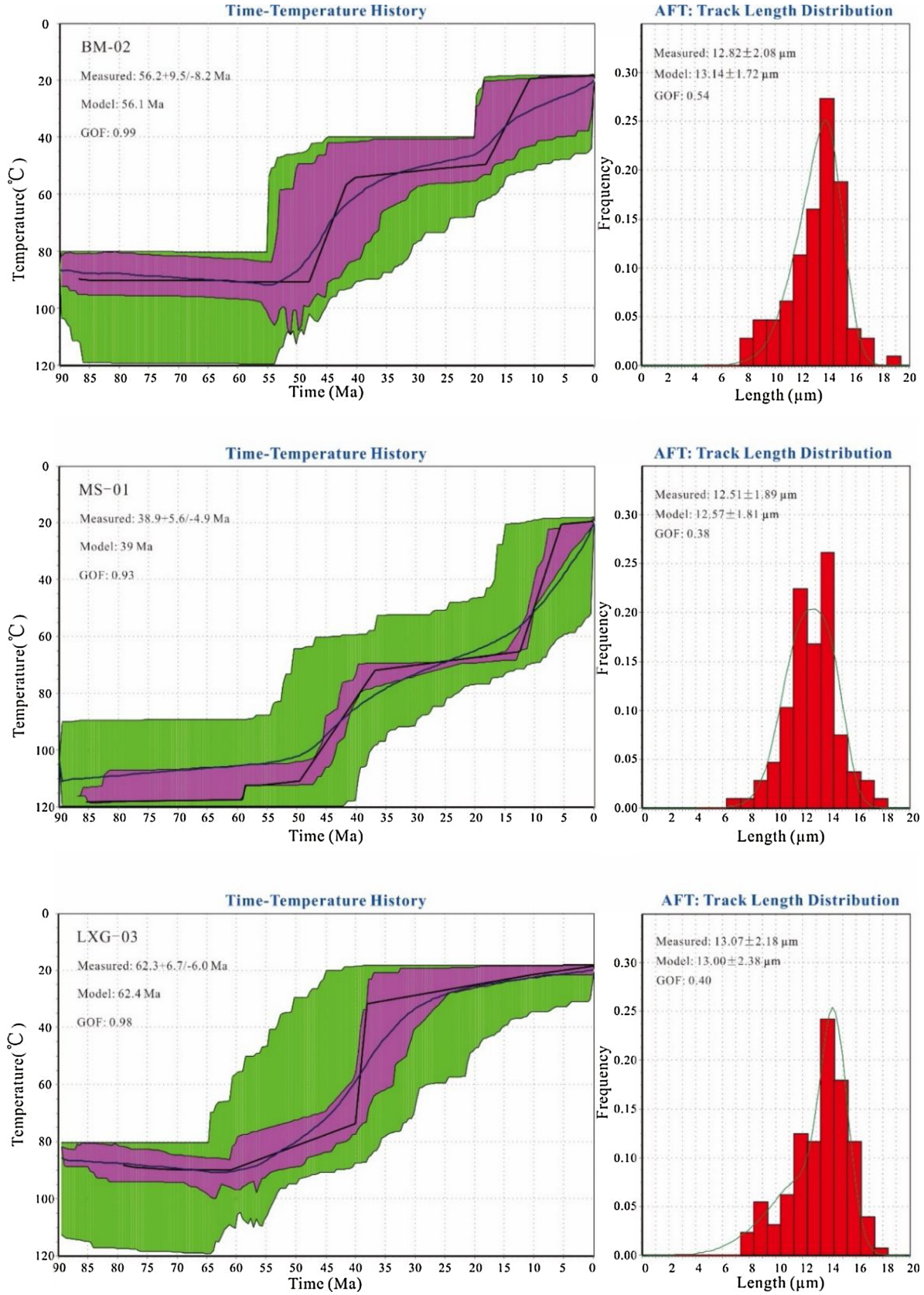

Fig. 7. Inverse modelling results of samples (BM-02, MS-01 and LXG-03) from the golden triangle region. The time-temperature paths based on the apatite fission-track data were made using the HeFty program (Ketchman, 2005). Present day temperature is set at 20 °C. The dark grey area corresponds to the range of good fits and the light grey area corresponds to the range of acceptable fits. The broken line represents the best fit. The curve represents the average fit. The Kolmogorov-Smirnov test was used to determine the goodness-of-fit (GOF) of the solutions to the real data.

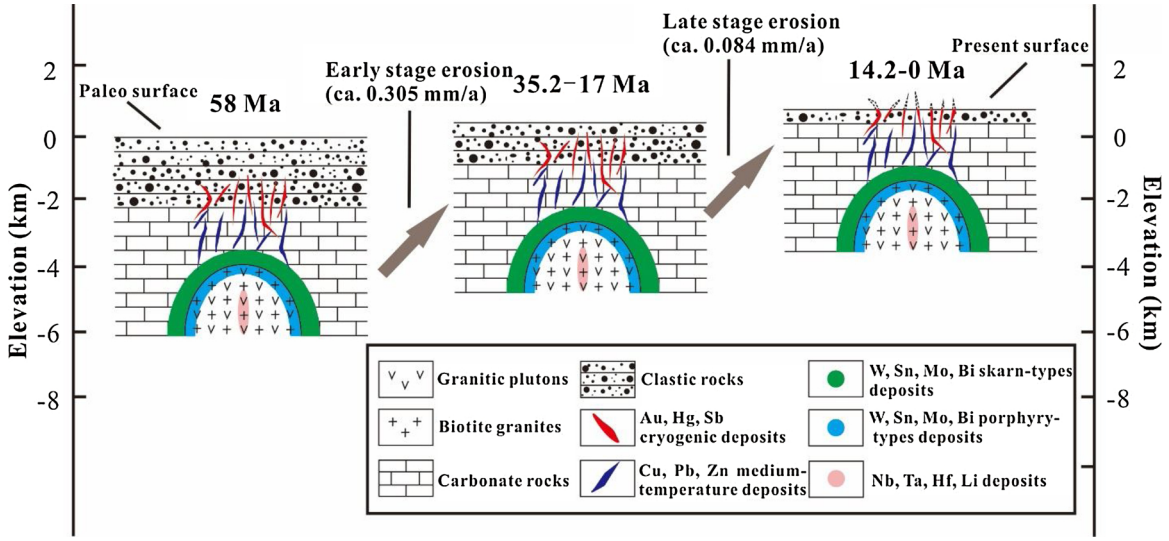

Fig. 8. Schematic diagram showing the uplift and denudation history of the Northwestern Guangxi. See text for details (modified from Leng et al., 2018).

Longxianggai pluton in Dachang of Guangxi. This is a relatively late magmatic activity developed in the background of the whole extensional tectonic environment in South China. We studied the diagenetic age of the Longxianggai rock mass, which confirms this viewpoint (Wu et al., 2020). In addition, this conclusion is also supported by previous studies (Wang et al., 2004; Liang et al., 2011; Cai et al., 2006; Li et al., 2008).

The collision between the Indian and Eurasian blocks was initiated ca. 60–40 Ma, resulting in the Himalayan orogeny (Zhou et al., 2018; Sun et al., 2016). The entire South China block was uplifted, as shown by the resulting accretion of the Asian continent, along with the rise of the Qinghai-Tibet Plateau, growth of fold-fault systems, and intrusion of intermediate–acid magma (Wang et al., 2002; Zhou et al., 2018). The Middle–Late Cretaceous–Tertiary South China basin formed as a lithospheric extensional structure, accompanied by regional-scale volcanic eruptions. The nature of this volcanic activity indicates a rapid shift from lower crust to upper mantle source magma in the early Eocene (about 56 Ma). This change was consequent to the extensional tectonics and thinning of the lithosphere of South China (Chung et al., 2005; Wu et al., 2008; Zhou et al., 2018; Jia et al., 2004), which also resulted in the uplift and denudation of the northwestern Guangxi. This geodynamic context is consistent with our apatite fission track simulations and age dating, which also suggest that the study area experienced a thermal event and rapid cooling during the period between 58 and 35.2 Ma (Figs. 6–8).

The results of thermal history modelling based on samples BM-02 and MS-01 indicate that the northwestern Guangxi area further underwent a stage of rapid cooling and subsequent thermal heating between 17 and 14.2 Ma (Figs. 6–8). The entire South China region experienced a period of rapid uplift induced by the rapid crustal wedging of the Indian plate during its collision with the Eurasian plate (Wrotel and Spakman, 2000; Oh, 2010; Jia et al., 2004). Intense deformation along fold-fault systems, magmatic activity, and metamorphism took place during this tectonic phase, which led to the development of numerous secondary faults as well as the overall uplift, erosion, and local tectonic inversion (Yi and Li, 1995). The concomitant occurrence of intense and extensive magmatic and tectonic activities caused the deformation and uplift of the Paleogene strata, enhancing the development of unconformities marking the contact with the overlying strata (Jia et al., 2004; Yi and Li, 1995). The exhumation event at 17–14.2 Ma was fundamental for the evolution of the Himalayan orogen, pattern of thrust-belt deformation, and geochemical evolution of the oceans.

6.2. *Preservation of hydrothermal deposits and metallogenic model*

Numerous studies have reported that the collision of the Indian and Asian blocks occurred between 60 and 40 Ma, resulting in the Himalayan orogeny and several phases of uplift (Sun et al., 2016; Zhou et al., 2018; Sorkhabi et al., 1994; Tapponnier et al., 2001; Chung et al., 2005; Wu et al., 2008; Wang et al., 2008). This is consistent with our apatite fission track simulations and age dating, indicating that the study area experienced a primary thermal event during the interval of 58–35.2 Ma (Figs. 6–8). Epithermal deposits, one of the most important types of gold mineralisation, are usually emplaced at depths of 2–3 km, making their preservation uncommon in ancient orogenic belts, which have long, complicated histories of exhumation (Wang and Groves, 2018). Previous studies have generally derived Mesozoic metallogenic ages for the Carlin-type gold deposits in the Golden Triangle region (Su et al., 1998; Su et al., 2009; Hu et al., 2017a,b; Pi et al., 2016, 2017; Chen et al., 2015, 2009). Understanding the preservation mechanism of these mineral deposits can thus offer valuable insights for ore exploration in ancient orogenic belts. The thermal and tectonic evolution of the northwestern Guangxi region since the late Yanshanian (90 Ma) can be regarded as a key to understanding the preservation of its epithermal deposits.

As discussed earlier, most of the Carlin-type gold deposits in the Golden Triangle region are considered to have formed in the Mesozoic. Fig. 7 shows that apatite fission track ages range between 81.6 Ma and 14.2 Ma and define three intervals: 81.6–77.1 Ma, 58–35.2 Ma, and 17–14.2 Ma. On this basis, the study area experienced three tectonic-thermal events. The late Yanshanian (90–70 Ma) was the late magmatic activity of the Longxianggai pluton (Wu et al., 2020). The early stage thermal event at 90–80 Ma is consistent with the age of formation of the main body of the Longxianggai pluton in Dachang, northwestern Guangxi. Furthermore, the age of the thermal event is also consistent with the Late Yanshanian (125–80 Ma) mineralisation of the Carlin-type gold deposit in the Golden Triangle (Yang et al., 2008; Cheng et al., 2010; Zhang et al., 2003; Liu and Hua, 2005; Hu and Zhou, 2012). Our apatite fission track data reveal a post-mineralisation thermal history since approximately 90 Ma. Two Carlin-type gold deposits, Bama and Mingshan, were found to have experienced exhumations of 2.037 km and 2.814 km, respectively, between 90 and 0 Ma. The Longxianggai complex pluton, which is closely related to the mineralisation of the Dachang Sn polymetallic ore field, experienced an exhumation of 1.986 km, similar to those of the Bama and Mingshan Carlin-type gold deposits.

The possible presence of granitic intrusions at depth in the Youjiang

Basin is inferred from geophysical evidence (Zhou, 1993). Zhou (1993) found that the gravity of the Youjiang Basin is high, reflecting the existence of the asthenosphere, slow crustal uplift, and deep concealed rock mass. The burial depth of the rock mass is closely related to the ore type and mineralisation temperature. Different depths represent different temperatures and favour different types of hydrothermal deposits. The area of ore-forming hydrothermal deposits shows a clear zoning with Nb, Ta, Hf, and Li from the inner to the outer contact zones of the rock. The transition zone is characterised by high temperature hydrothermal deposits such as W, Sn, Mo, and Bi, and medium-temperature deposits such as Cu, Pb and Zn. The middle and outer zones are characterised by Au, Hg, and Sb cryogenic deposits (Cen and Tian, 2012; Zhang et al., 2012; Mao et al., 2010).

In addition to the geophysical evidence, the geology of the Bama Carlin-type gold deposit area also supports this interpretation. This deposit is located at the southwest limit between the basin and the intra-oceanic carbonate platform along the Longtian anticline structure (Li et al., 2014b). This area underwent a multi-phase tectonic activity that resulted in intense deformation and the development of relevant folds and faults, producing joints, fissures, and cleavages in the strata. At present, 9 faults (numbered F_1 to F_9) have been identified in the mining area, some trending mainly NW (F_1, F_2, F_3, F_4) and others nearly EW (F_5, F_6, F_8, F_9). These faults exert a direct control on mineralisation processes, as evidenced by the close position and distribution of the ore bodies. In particular, F_1 and F_2 are synsedimentary faults, whereas F_3, F_4, F_5, F_6 and F_9 are ore-controlling and ore-bearing faults in the mining area (Li et al., 2014b) (Fig. 3). In addition, two quartz porphyry dykes in the mining area show a NE strike (Fig. 3). Therefore, these faults provide favourable conditions for the penetration of ore-forming deposits and the intrusion of deep-seated magma. The Mingshan Carlin type gold deposit features two groups of faults trending NW and NE. The ore body is mainly accommodated along the fracture zones of the overall NW oriented faults and associated secondary structures. Ore body No. 2, for instance, is mainly controlled by the F_2 fault zone (Pang et al., 2014). In addition, Yanshanian quartz porphyry occur in the northern and eastern sectors of the mining area (Pang et al., 2014). Based on hydrogen, oxygen and argon isotopes present in the fluid inclusions as well as the chemical composition of the quartz porphyry, mineralisation can be correlated with magmatic activity (Pang et al., 2014). Similar to the previous, also these faults provide preferential pathways for the penetration of ore-forming elements and the intrusion of deep-seated magma.

Based on the inference of deep-seated concealed rock masses, apatite fission track thermal history simulation, and geological and geochemical characteristics, the following metallogenic model was derived (Fig. 8). Subsequent to the culmination of the collision between the Indian and Eurasian blocks, northwestern Guangxi entered a period of rapid uplift, with a number of denudations at 60–40 Ma (Zhou et al., 2018; Sun et al., 2016; Wang et al., 2002). Following this period, there was a phase of rapid ascent at about 20 Ma, indicating intense magmatic activity. Due to the rapid wedging of the Indian plate against the Eurasian plate, the entire South China region entered a period of rapid uplift (Jia et al., 2004). The progressing of uplift enhanced the denudation of a large number of low-temperature deposits and the exhumation of mid–high temperature hydrothermal deposits. Although some Carlin-type gold deposits are preserved in the Golden Triangle region, others have been denuded during the proposed phases, as presented in the reconstructed thermal history herein. Some low-temperature Au, Hg and Sb deposits, similar to the Carlin-type gold deposits, may have been denuded to varying degrees (Fig. 8). This also explains why the Carlin-type gold deposits in northwestern Guangxi show small–medium sized deposits and some mineralisation points (Fig. 2). Our sampling site in the Dachang tin polymetallic ore field represents a typical ultra-large high-temperature hydrothermal tin ore field (Chen et al., 1993; Li et al., 2008; Pi et al., 2015; Liang et al., 2011). This evidence, combined with our apatite fission track thermal history modelling, suggests that the above medium–low temperature deposit has been likely denuded. Some authors have proposed that medium-high temperature deposits are present in South China (Hu et al., 2017b; Qiu et al., 2014). Accordingly, we surmise that some hydrothermal deposits, such as medium-temperature Cu, Pb, Zn deposits and high-temperature W, Sn, Mo, Bi deposits, or polymetallic Cu–Fe–Mo and Cu–Mo–(Pb–Zn) porphyry types and skarn types, may be buried below some of the low-temperature Carlin-type gold deposits. Alternatively, similar deposits may occur at variable depths in northwestern Guangxi. Considering the effect of erosion, transport, and deposition, sand gold deposits may be an important prospecting target.

7. Conclusions

Apatite fission track dating combined with thermal history modelling revealed the multiple tectono-thermal events leading to the conservation of hydrothermal deposits in northwestern Guangxi.

1 Based on fission-tracks with mean lengths ranging from 12.3 ± 2.6 μm to 14.4 ± 0.5 μm, six new apatite fission track ages ranging from 81.6 Ma to 14.2 Ma were obtained from apatite samples collected in different areas of northwestern Guangxi. These ages defined three distinct time intervals: 81.6–77.1 Ma, 58–35.2 Ma, and 17–14.2 Ma, corresponding to three tectono-thermal events in northwestern Guangxi. The results indicate a total exhumation of 2–3 km since the late Yanshanian (90 Ma) in northwestern Guangxi.
2 According to our new apatite fission track data, the 81.6–77.1 Ma event represents a period of magmatic activity in northwestern Guangxi. The first phase of the early Himalayan tectonic movement was caused by the subduction–collision of the Indian and Asian plates at ca. 58–35.2 Ma. The second phase is attributable to the rapid wedging of the Indian plate at 17–14.2 Ma.
3 We surmise that some hydrothermal deposits, including medium-temperature Cu, Pb, Zn deposits and high-temperature W, Sn, Mo, Bi deposits such as polymetallic Cu–Fe–Mo, and Cu–Mo–(Pb–Zn) porphyry types and skarn types, may be locally present below the low-temperature Carlin-type gold deposits, or at variable depths in northwestern Guangxi. Considering that sediments from the Carlin-type gold ore are eroded and transported by rivers, sand gold deposits may be a relevant prospecting target.

CRediT authorship contribution statement

Wu Jianbiao: Conceptualization, Software, Investigation, Data curation, Writing - original draft, Validation. **Pi Qiaohui:** Validation, Methodology, Investigation, Formal analysis, Visualization, Supervision. **Zhu Bin:** Validation, Formal analysis, Investigation. **Hu Yunhu:** Validation, Formal analysis, Investigation. **Li Guo:** Investigation, Writing - review & editing, Validation. **Wei Chaowen:** Investigation, Writing - review & editing, Validation.

Declaration of Competing Interest

None.

Acknowledgement

This work was financed jointly by the National Natural Science Foundation of China (Grant No. 41973042), Guangxi Natural Science Foundation (2016GXNSFGA380004, 2017JJA140081), and the Fifth Bagui Scholar Innovation Project of Guangxi Province (to XU Ji-feng). We gratefully acknowledge supports from Elsevier's Language Editing Service and EditSprings for their contributions in improving the manuscript and the English language review.

References

Brandon, M.T., 1996. Probability density plot for fission-track grain-age samples. Radiat. Meas. 26 (5), 663–676.

Cai, M.H., He, L.Q., Liu, G.Q., Wu, D.C., Huang, H.M., 2006. SHRIMP zircon U-Pb dating of the intrusive rocks in the Dachang tinpolymetallic ore field, Guangxi and their geological significance. Geol. Rev. 52 (3), 409–414 (in Chinese with English abstract).

Cai, J.X., Zhang, K.J., 2009. A new model for the Indochina and South China collision during the Late Permian to the Middle Triassic. Tectonophysics 469, 35–45.

Cen, K., Tian, Z.X., 2012. Ore-forming system around magma — model of spatial zonation for magmatic rock and deposit set. Geoscience 26 (5), 1051–1057 (in Chinese with English abstract).

Chen, Y.C., Huang, M.Z., Xu, J., Hu, Y.Z., Tang, S.H., Li, Y.Q., Meng, L.K., 1993. Tin Deposits of Dachang. Geological Publishing House, Beijing.

Chen, M.H., Huang, Q.W., Hu, Y., Chen, Z.Y., Zhang, W., 2009. Genetic types of phyllosilicate (micas) and its ^{39}Ar-^{40}Ar dating in Lannigou gold deposit, Guizhou Province, China. Acta Min. Sin. 29, 353–362 (in Chinese with English abstract).

Chen, M.H., Lu, G., Li, X.H., 2012. Muscovite ^{40}Ar/^{39}Ar dating of the quartz porphyry veins from Northwest Guangxi, China, and its geological significance. Geol. J. China Univ. 18 (1), 106–116.

Chen, M.H., Zhang, Y., Meng, Y.Y., Lu, G., Liu, S.Q., 2014. Determination of upper limit of metallogenic epoch of Liaotun gold deposit in western Guangxi and its implications for chronology of Carlin-type gold deposits in Yunnan-Guizhou-Guangxi “golden triangle” area. Min. Depos. 33 (1), 1–13 (in Chinese with English abstract).

Chen, M.H., Mao, J.W., Li, C., Zhang, Z.Q., Dang, Y., 2015. Re-Os isochron ages for arsenopyrite from Carlin-like gold deposits in the Yunnan-Guizhou-Guangxi “golden triangle”, southwestern China. Ore Geol. Rev. 64, 316–327.

Cheng, Y.B., Tong, X., Wu, J.D., Mo, G.P., 2010. Geochronology framework of the W-Sn mineralization granites in western South China and their geological significance. Acta Petrol. Sin. 26, 809–818 (in Chinese with English abstract).

Chung, S.L., Chu, M.F., Zhang, Y.Q., Xie, Y.Q., Lo, C.H., Lee, T.Y., Lan, C.Y., Li, X.H., Zhang, Q., Wang, Y.Z., 2005. Tibetan tectonic evolution inferred from spatial and temporal variations in post-collisional magmatism. Earth. Rev. 68, 173–196.

Faure, M., Lepvrier, C., Nguyen, V.V., Vu, T.V., Lin, W., Chen, Z., 2014. The South China block-Indochina collision: where, when, and how? J. Asian Earth Sci. 79, 260–274.

Feng, Y.L., Yuan, W.M., Tian, Y.T., Feng, X., Hao, N.N., Zhang, L.T., Li, Y.H., Liu, Q.S., Wang, X.L., Zhen, S.Z., Zhu, X.Y., Wang, K., 2017. Preservation and exhumation history of the harizha-halongxiuma mining area in the East Kunlun Range, northeastern Tibetan Plateau, China. Ore Geol. Rev. 90, 1018–1031.

Gao, P., Zheng, Y.F., Zhao, Z.F., 2016. Distinction between S-type and peraluminousI-type granites: zircon versus whole-rock geochemistry. Lithos 258, 77–91.

Green, P.F., 1981. A new look at statistics in fission-track dating. Nucl. Tracks 5, 77–86.

Guo, J.H., 1994. The metallogenetically geological conditions and prospecting model of the super micrograined disseminated-type gold deposits in Northwestern Guangxi. Guangxi Geo. 7 (2), 37–50 (in Chinese with English abstract).

Guo, J., Zhang, R.Q., Sun, W.D., Ling, M.X., Hu, Y.B., Wu, K., Ming, L.C., Zhang, L., 2018. Genesis of tin-dominant polymetallic deposits in the Dachang district, South China: Insights from cassiterite U–Pb ages and trace element compositions. Ore Geol. Rev. 95, 863–879.

Hu, R.Z., Su, W.C., Bi, X.W., Li, Z.Q., 1995. A possible evolution way of oreforming hydrothermal fluid for the Carlin-type gold deposits in the Yunnan-Guizhou-Guangxi triangle area. Acta Min. Sin. 15, 144–149 (in Chinese with English abstract).

Hu, R.Z., Su, W.C., Bi, X.W., Tu, G.Z., Hofstra, A.H., 2002. Geology and geochemistry of Carlin-type gold deposits in China. Min. Depos. 37, 378–392.

Hu, R.Z., Mao, J.W., Fan, W.M., Hua, R.M., Bi, X.W., Zhong, H., Song, X.Y., Tao, Y., 2010. Some scientific questions on the intra-continental metallogeny in the South China continent. Earth Sci. Front. 17 (2), 013–026 (in Chinese with English abstract).

Hu, R.Z., Fu, S.L., Huang, Y., Zhou, M.F., Fu, S.H., Zhao, C.H., Wang, Y.J., Bi, X.W., Xiao, J.F., 2017a. The giant South China Mesozoic low-temperature metallogenic domain: reviews and a new geodynamic model. J. Asian Earth Sci. 137, 9–34.

Hu, R.Z., Chen, W.T., Xu, D.R., Zhou, M.F., 2017b. Reviews and new metallogenic models of mineral deposits in South China: an introduction. J. Asian Earth Sci. 137, 1–8.

Hu, R.Z., Zhou, M.F., 2012. Multiple Mesozoic mineralization events in South China an introduction to the thematic issue. Min. Depos. 47, 579–588 (in Chinese with English abstract).

Jia, D.C., Hu, R.Z., 2001. Analysis of genesis of carlin-type gold deposits in Yunnan-Guizhou-Guangxi Triangle Area. Min. depos. 20 (4), 378–384 (in Chinese with English abstract).

Jia, C.Z., He, D.F., Lu, J.M., 2004. Episodes and geodynamic setting of Himalayan movement in China. Oil Gas Geol. 2 121–125+169 (in Chinese with English abstract).

Kesler, S.E., Riciputi, L.C., Ye, Z.J., 2005. Evidence for amagmatic origin for Carlin-type gold deposits: isotopic composition of sulfur in the Betze-post-screamer deposit, Nevada, USA. Min. Depos. 40, 127–136.

Ketchman, R.A., 2005. Forward and inverse modeling of low-temperature thermochronometry data. Rev. Min. Geochem. 58, 275–314.

Lei, Y.L., Zhong, D.L., Jia, C.Z., Ji, J.Q., 2008. Late Cenozoic differential uplift-exhumation of batholith and propagation of uplift recorded by fission track thermochronology in Chayu area, the southeast margin of the Tibetan plateau. Acta Petrolog. Sin. 24 (2), 384–394.

Leng, C.B., Cooke, D.R., Hou, Z.Q., Evans, J.E., Zhang, X.C., Chen, W.T., Danišík, M., McInnes, B.I.A., Yang, J.H., 2018. Quantifying exhumation at the giant pulang porphyry Cu-Au deposit using U-Pb-He dating. Econ. Geol. 113 (5), 1077–1092.

Lepvrier, C., Faure, M., Voung, N.V., Tich, V.V., Lin, W., Thang, T.T., Phuong, T.H., 2011. North-directed Triassic nappes in Northeastern Vietnam (East Bac Bo). J. Asian Earth Sci. 41, 56–68.

Li, S.R., Wang, D.H., Liang, T., Qu, W.J., Ying, L.J., 2008. Metallogenic epochs of the Damingshan tungsten deposit in Guangxi and its prospecting potential. Acta Geol. Sin. 82 (7), 873–879 (in Chinese with English abstract).

Li, X.Y., Zheng, J.P., Ma, Q., Xiong, Q., Griffin, W.L., Lu, J.G., 2014a. From enriched to depleted mantle: evidence from Cretaceous lamprophyres and Paleogene basaltic rocks in eastern and central Guangxi Province, western Cathaysia block of South China. Lithos. 184, 300–313.

Li, Y.Q., Pang, B.Q., Yang, F., Zhang, D.L., Zeng, Q.F., Liu, X., Jiang, X.H., 2014b. Geochemical Characteristics and Metallogenic Significance of Quart Porphyry in Liaotun Gold Deposit, Bama County, Guangxi. Geosci. 28 (6), 1138–1150 (in Chinese with English abstract).

Li, Y.Q., Pang, B.Q., Xiao, H., Zhou, Y.Q., Lv, J.W., Lai, X., 2015. Isotopic geochemistry analysis of carlin-type gold deposits in Minshan, Northwest Guangx. Acta Min. Sin. 35 (S1), 224–225.

Liang, T., Wang, D.H., Hou, K.J., Li, H.Q., Huang, H.M., Cai, M.H., Wang, D.M., 2011. LA-MC-ICP-MS zircon U-Pb dating of Longxianggai pluton in Dachang of Guangxi and its geological significance. Acta Petrol. Sin. 27 (6), 1624–1636 (in Chinese with English abstract).

Liu, X.D., Hua, R.M., 2005. ^{40}Ar/^{39}Ar dating of adularia from the Bitian gold-silver-copper deposit, Fujian Province. Geol. Rev. 51, 151–155 (in Chinese with English abstract).

Mao, J.W., Xie, G.Q., Li, X.F., Zhang, C.Q., Mei, Y.X., 2004. Mesozoic large-scale mineralization and multiple lithospheric extension in South China. Earth Sci. Front. 11 (1), 45–55.

Mao, J.W., Zhang, J.D., Guo, C.l., 2010. Porphyry Cu, epithermal Ag-Pb-Zn, distal hydrothermal Au deposits: a new model of mineral deposit——taking the Dexing area as an example. J. Earth Sci. Environ. Stud. 32 (1), 1–14 (in Chinese with English abstract).

Mao, J.W., Cheng, Y.B., Chen, M.H., Pirajno, F., 2012. Major types and time-space distribution of Mesozoic ore deposits in South China and their geodynamic settings. Miner. Depos. 48, 267–294.

Oh, C.W., 2010. Systematic changes in metamorphic styles along the Dabie-Hongseong and Himalayan collision belts, and their tectonic implications. J. Asian Earth Sci. 39 (6), 635–644.

Pang, B.C., Xiao, H., Fu, W., Zhang, Q.W., Chen, H.Y., 2014. Microfabric and composition of hydrothermal minerals from the Mingshan Carlin gold deposit in Northwestern Guangxi and their implication for ore-forming process. J. Jilin Univ.: Earth Sci. Ed. 44 (1), 105–119 (in Chinese with English abstract).

Peng, Y., Lu, G., 2019. Study on buttress unconformity in Late Palaeozoic carbonatesof northwestern Guangxi. Geol. Rev. 65 (4), 754–809 (in Chinese with English abstract).

Peng, J.T., Hu, R.Z., Burnard, P.G., 2003. Samarium-neodymium isotope systematics of-hydrothermal calcites from the Xikuangshan antimony deposit (Hunan, China): thepotential of calcite as a geochronometer. Chem. Geol. 200, 129–136.

Pi, Q.H., Hu, R.Z., Wang, D.H., Miao, B.K., Qin, X.F., Chen, H.Y., 2015. Enrichment of indium in west ore belt of Dachang ore field: evidence from ore textures and sphalerite geochemistry. Min. Depos. 34 (2), 379–396 (in Chinese with English abstract).

Pi, Q.H., Hu, R.Z., Peng, K.Q., Wu, J.B., Wei, C.W., Huang, Y., 2016. Geochronology of the Zhesang gold deposit and mafic rock in Funing County of Yunnan Province, with special reference to the dynamic background of Carlin-type gold deposits in the Dian-Qian-Gui region. Acta Petrol. Sin. 32 (11), 3331–3342 (in Chinese with English abstract).

Pi, Q.H., Hu, R.Z., Xiong, B., Li, Q.L., Zhong, R.C., 2017. In situ SIMS U-Pb dating of hydrothermal rutile: reliable age for the Zhesang Carlin-type gold deposit in the golden triangle region, SW China. Min. Depos. 52, 1179–1190.

Piedrahita, V.A., Bernet, M., Chadima, M., Sierra, G.M., Marín-Cerón, M.I., Toro, G.E., 2017. Detrital zircon fission-track thermochronology and magnetic fabric of the Amagá Formation (Colombia): intracontinental deformation and exhumation events in the northwestern Andes. Sediment. Geol. 356, 26–42.

Qiu, L., Yan, D.P., Zhou, M.F., Arndt, N.T., Tang, S.L., Qi, L., 2014. Geochronology and geochemistry of the Late Triassic Longtan pluton in South China: termination of the crustal melting and Indosinian orogenesis. Int. J. Earth Sci. 103 (3), 649–666.

Qiu, L., Yan, D.P., Tang, S.L., Wang, Q., Yang, W.X., Tang, X.L., Wang, J.B., 2016. Mesozoic geology of southwestern China: indosinian foreland overthrusting and subsequent deformation. J. Asian Earth Sci. 122, 91–105.

Sorkhabi, R.B., Jain, A.K., Nishimura, S., Itaya, T., Lal, N., Manickavasagam, R.M., Tagami, T., 1994. New age constraints on the cooling and unroofing history of the Trans-Himalayan Ladakh Batholith (Kargil area), NW India. Proc. Indian Acad. Sci. (Earth Planet. Sci.). 103, 83–97.

Su, W.C., Yang, K.Y., Hu, R.Z., Chen, F., 1998. Fluid inclusion chronological study of the Carlin-type gold deposits in southwestern China: as exemplified by the Lannigou gold deposit, Guizhou province. Acta Min. Sin. 18 (3), 359–362 (in Chinese with English abstract).

Su, W.C., Hu, R.Z., Xia, B., Xia, Y., Liu, Y.P., 2009. Calcite Sm-Nd isochron age of the Shuiyindong Carlin-type gold deposit, Guizhou, China. Chem. Geol. 258 (3–4), 269–274.

Sun, X.M., Wei, H.X., Zhai, W., Shi, G.Y., Liang, Y.H., Mo, R.W., Han, M.X., Yi, J.Z., Zhang, X.G., 2016. Fluid inclusion geochemistry and Ar-Ar geochronology of the Cenozoic Bangbu orogenic gold deposit, southern Tibet, China. Ore Geol. Rev. 74, 196–210.

Tang, Y., Zhang, Y.P., Tong, L.L., 2018. Mesozoic-Cenozoic evolution of the Zoige depression in the Songpan-Ganzi flysch basin, eastern Tibetan Plateau: constraints from detrital zircon U-Pb ages and fission-track ages of the Triassic sedimentary sequence. J. Asian Earth Sci. 151, 285–300.

Tapponnier, P., Xu, Z.Q., Roger, F., Yang, J.S., 2001. Geology-oblique stepwise rise and

growth of the Tibet plateau. Science 294, 1671–1677.
Vermeesch, P., 2009. Radial Plotter: a Java application for fission track, luminescence and other radial plots. Radiat. Meas. 44 (4), 409–410.
Wang, Q.F., Groves, D., 2018. Carlin-style gold deposits, Youjiang Basin, China: tectono-thermal and structural analogues of the Carlin-type gold deposits, Nevada, USA. Miner. Depos. 53 (7), 909–918.
Wang, J., Huang, S.Y., Huang, G.H., Wang, J.J., 1986. Basic characteristics of the earth's temperature distribution in southern China. Acta Geol. Sin. 3, 297–310 (in Chinese with English abstract).
Wang, C.S., Liu, Z.F., Li, X.H., 2002. The subduction of Paleo-Tethys, continental collision, plateau uplift and sedimentary response. In: Chen, Y.C. (Ed.), The 80th Anniversary academic Proceedings of the Chinese Geological Society, pp. 162–172 (in Chinese with English abstract).
Wang, D.H., Chen, Y.C., Chen, W., Sang, H.Q., Li, H.Q., Lu, Y.F., Chen, K.L., Lin, Z.M., 2004. Dating the Dachang giant tin-polymentallic deposit in Nandan, Guangxi. Acta Geol. Sin. 78 (1), 132–133 (in Chinese with English abstract).
Wang, Y.J., Fan, W.M., Cawood, P.A., Ji, S.C., Peng, T.P., Chen, X.Y., 2007. Indosinian high-strain deformation for the Yunkaidashan tectonic belt, South China: kinematics and $^{40}Ar/^{39}Ar$ geochronological constraints. Tectonics 26 (6).
Wang, C.S., Zhao, X.X., Liu, Z.F., Lippert, P.C., Graham, S.A., Coe, R.S., Yi, H.S., Zhu, L.D., Liu, S., Li, Y.L., 2008. Constraints on the early uplift history of the Tibetan Plateau. Proc. Natl. Acad. Sci. U. S. A. 105, 4987–4992.
Wang, Z.P., Xia, Y., Song, X.Y., Liu, J.Z., Yang, C.F., Yan, B.W., 2013. Study on the evolution of ore-formation fluids for Au-Sb ore deposits and the mechanism of Au-Sb paragenesis and differentiation in the southwestern part of Guizhou Province, China. Chin. J. Geochem. 32, 56–68.
Wang, X., Deng, L., Zattin, M., Ji, M., Li, J., 2017. Palaeogene growth of the northeastern Tibetan Plateau: detrital fission track and sedimentary analysis of the Lanzhou basin, NW China. J. Asian Earth Sci. 147, 322–331.
Wrotel, M.J.R., Spakman, W., 2000. Subduction and slab detachment in the Mediterranean-Carpathian region. Science 290, 1910–1917.
Wu, F.Y., Huang, B.C., Ye, K., Fang, A.M., 2008. Collapsed Himalayan-Tibetan orogeny and the rising Tibetan plateau. Acta Petrol. Sin. 23, 1–30 (in Chinese with English abstract).
Wu, J.B., Hu, Y.H., Pi, Q.H., Wei, C.W., Li, G., Yang, X., Yang, H.L., Yu, H.D., Lu, D., 2020. Zircon fission track (ZFT) age of the Longxianggai pluton in Dachang of Guangxi and its geological significance. Geol. Bull. China 39 (4), 512–522 (in Chinese with English abstract).
Yang, Z.X., Mao, J.W., Chen, M.H., Tong, X., Wu, J.D., Cheng, Y.B., Zhao, H.J., 2008. Re-Os dating of molybdenites from the Kafang skarn copper (tin) deposit in the Gejiu tin polymetallic ore district and its geological significance. Acta Petrol. Sin. 24, 1937–1944 (in Chinese with English abstract).
Yang, J.H., Cawood, P.A., Du, Y.S., Huang, H., Hu, L.S., 2012. Detrital record of Indosinian mountain building in SW China: provenance of the Middle Triassic turbidites in the Youjiang Basin. Tectonophysics 574, 105–117.
Yi, M.C., Li, X., 1995. Division of crustal movement of Himalayan period in Yanshan area and its expressed features. Geoscience 9 (3), 325–326 (in Chinese with English abstract).
Yuan, W.M., 2016. Thermochronological method of revealing conservation and changes of mineral deposits. Acta Petrol. Sin. 32 (8), 2571–2578 (in Chinese with English abstract).
Yuan, W.M., Deng, J., Zheng, Q.G., Dong, J.Q., Bao, Z.K., Eizenhoefer, P.R., Xu, X.T., Huang, Z.X., 2009. Apatite fission track constraints on the Neogene tectono-thermal history of Nimu area, southern Gangdese terrane, Tibet Plateau. Isl. Arc 18, 488–495.
Zhang, F., Yang, K.Y., 1992. Study on the fission track metallogenic age of micro disseminated gold deposits in Southwest Guizhou. Chinese Sci. Bull. 27 (17), 1593–1595 (in Chinese with English abstract).
Zhang, D.Q., Feng, C.Y., Li, D.X., She, H.Q., Dong, Y.J., 2003. ^{40}Ar-^{39}Ar dating of adularia from Bitian sericite-adularia type epithermal Ag-Au deposit in Fujian Province and its geological significance. Min. Depos. 22, 360–364 (in Chinese with English abstract).
Zhang, C.Q., Wang, D.H., Wang, Y.L., Wang, C.H., Qiu, X.P., 2012. Discuss on the metallogenic model for Gaolong gold deposit in Tianlin County, Guangxi, China. Acta Petrol. Sin. 28 (1), 213–224 (in Chinese with English abstract).
Zhang, N., Huang, Q.M., Tan, J.Z., Li, J., 2016. Extensive structural characteristics of Youjiang Basin, western Guangxi. Geol. China 43 (3), 953–968 (in Chinese with English abstract).
Zhou, Y.F., 1993. The application of regional gravity to the deep geology and mineralization prognosis in Guangxi. Geol. Guangxi. 6, 15–24 (in Chinese with English abstract).
Zhou, Q., Sun, H.S., Evans, N., Li, C., Liu, Z., Zhang, Q.C., Huang, J.H., 2018. Contemporaneous east-west extension and north-south compression at 43 Ma in the Himalayan orogen. J. Struct. Geol. 117, 124–135.
Zhu, L.M., Liu, X.F., Jin, J.F., He, M.Y., 1998. The study of the time-space distribution and source of ore-forming fluid for the fine-disseminated gold deposits in the Yunnan-Guizhou-Guangxi area. Sci. Geol. Sin. 33 (4), 82–93 (in Chinese with English abstract).